13th International Symposium on Turbulence and Shear Flow Phenomena (TSFP13)
Montreal, Canada, June 25–28, 2024

THE EFFECTS OF TURBULENCE AND SURFACE CAPILLARY WAVES ON OXYGEN TRANSFER ACROSS AN AIR-WATER INTERFACE

Leon Li
Department of Energy & Process Engineering
Norwegian University of Science & Technology
Kolbjørn Hejes vei 2, 7034 Trondheim, Norway
leon.li@ntnu.no

Pim A. Bullee
Institute of Fluid Dynamics
ETH Zürich
Sonneggstrasse 3, 8092 Zürich, Switzerland
pbullee@ethz.ch

R. Jason Hearst
Department of Energy & Process Engineering
Norwegian University of Science & Technology
Kolbjørn Hejes vei 2, 7034 Trondheim, Norway
jason.hearst@ntnu.no

ABSTRACT

An experimental study is performed to investigate the separate influences of bulk turbulence and surface capillary waves on the gas transfer velocity of atmospheric oxygen into a body of water. Through the combination of an active grid and an array of surface penetrating dowels, we are able to create flow cases with similar surface wave characteristics but different bulk turbulence properties and vice versa, thus enabling separated investigations into the effects of these two factors on the gas transfer velocity, k. We found that while both the presence of surface capillary waves and elevated bulk turbulence lead to faster gas transfer, evidence points to the bulk turbulence as having the greater impact on k. We use both U_τ along the channel floor and an averaged bulk turbulence intensity to characterise the bulk turbulence and found that both quantities have a strong correlation with k, whereas the correlation of k with the surface wave characteristics is weaker.

INTRODUCTION

The concentration of low solubility gas species in water, such as O_2 and CO_2, plays an important role for the climate and the biosphere of the Earth. For example, having an accurate understanding of oceanic carbon capture leads to better predictions for climate models. In a recent review of the current state in estimating the air-sea flux of CO_2, the uncertainty in estimating the gas transfer velocity, k, is identified as the largest contributor to the overall uncertainty in estimating the flux (Woolf *et al.*, 2019). Thus, having an accurate understanding of the behaviour of k when influenced by various external factors is the overall motivation for this work.

One model for k proposes that at the surface in the liquid phase, a thin film exists in which gas transfer from the air to water is dominated by molecular diffusion. For gases with low solubility, this is the bottleneck in the process and can wholly influence k (Kanwisher, 1963*a*,*b*). This thin film, however, can become distorted by interfacial deformation such as gravity and capillary waves. In the past decades, multiple studies have focused on the effects of capillary waves on the values for k for different gas species. MacIntyre (1971) predicted that k can increase by a factor of up to 3.5 due to the thinning of the film layer caused by the periodic surface dilation from the capillary waves. They further suggested that this effect is independent of the film thinning due to bulk turbulence. Likewise, heat transport can also be enhanced across the air-water interface by the presence of capillary waves (Witting, 1971). Increased sub-surface vorticity from cumulative shedding from the capillary waves has also been suggested as a cause for the increase in k (Longuet-Higgins, 1992). Szeri (1997) predicts a three-fold increase in k for reacting flows that remove the dissolved gas from the thin film. However, when the same model is applied to non- or weakly reacting flows, the predicted increase in k is negligible.

Several experiments have been conducted to test the validity of these predictions with varying degrees of success. Kanwisher (1963*a*,*b*) found that wind generated capillary-gravity waves can lead to an order of magnitude increase in k, at wind speeds up to 10 ms^{-1}. Although they did not characterise the wave topology, strong correlations were found between the onset of capillary waves and an increase in k. This increase, however, is much higher than any of the aforementioned models predicted. Likewise, Liss (1973) and Coantic (1986) also reported up to an order of magnitude increase in k due to wind driven surface waves. Qualitatively, the three aforementioned studies showed that k increases as the square of the wind speed beyond the initial onset of capillary waves. Relating the wave topology to k, Jähne *et al.* (1987) saw that k correlates well with the mean square of the wave slope for wind-driven waves. Furthermore, they showed that one should consider the statistics of the whole wave topology of the wind generated capillary-gravity waves, and not just the small scale parasitic capillary waves proposed by Coantic (1986). This relation between k and the wave slope is replicated later in a small water reservoir with Faraday waves by Saylor & Handler (1997, 1999), as opposed to the wind generated waves from the previous experiments in an effort to eliminate any turbulence effects caused by the wind shear. The Faraday waves saw an increase of two orders of magnitude in k, which is much higher than what is predicted by the available models. Interestingly, surfactants play no significant role in the behaviour of k if the resulting waves have similar mean square slopes (Saylor

& Handler, 1999). More recently, Adler (2022) used an array of shallow penetrating dowels to generate surface capillary-gravity waves, and saw a six-fold increase in k in some test cases. In all of these experimental studies, there is indeed a strong correlation between k and the surface wave topology. However, it must be pointed out that the experimental results in large greatly overshoots the predicted increment in k, and furthermore, there is no characterisation of the bulk flow in the liquid phase to show that the increase in k is isolated to be from the effects of the surface waves alone. Indeed, Henstock & Hanratty (1979) concede that it is difficult to distinguish the effects of turbulence and waves. It is clear that both the models and the experiments need further development.

Danckwerts (1951) suggested that another model should be used to explain the increase in k when there is bulk turbulence in either or both phases, namely the surface renewal model. Parcels of fresh, unsaturated bulk fluid are continuously transported to the surface, where they can rapidly absorb gas species from the air, before being replenished by new fluid parcels. It is argued that this should be the dominant process that controls the overall mass flux in a flow with non-negligible bulk turbulence. The gas transfer velocity would therefore depend on the frequency of the renewal events, which would be generally faster in flows with higher degrees of bulk turbulence. On top of the surface renewal events, Kanwisher (1963*a*,*b*) also found that bulk turbulence, in a separate stirring experiment, can modify the thickness of the surface boundary layer, thereby also influencing the thin-film model. Along the same vein, Szeri (1997) proposed adding a pre-factor to the surface renewal model that is based on wave amplitude to account for enhancement from capillary waves. The pre-factor gives a 70% enhancement to the predictions of Danckwerts (1951). Moving to the actual turbulence mechanisms responsible, the convective motions of the two phases close to the interface alone cannot adequately explain the enhancement in k. It rather requires characterisations with multi-scales structures that are more associated with the bulk turbulence properties (Henstock & Hanratty, 1979). Some suggest that mass transfer is controlled by the flow fluctuations in the gas phase, which imprints its effects on the surface capillary waves (e.g. McCready & Hanratty, 1985; Komori *et al.*, 1993), while others argued that the dominant effects due to turbulence are in the liquid phase (Coantic, 1986; Jähne *et al.*, 1987). Regardless of which phase is dominant, Komori *et al.* (1993) produced mass transfer rates agreeing well with the surface renewal model. Adding further supportive evidence, k can increase significantly with bulk velocity fluctuations alone, as shown in several zero-mean flow stirred tank experiments, where there were minimal distortions to the surface topology (Herlina & Jirka, 2008; Jirka *et al.*, 2010; Variano & Cowen, 2013).

It would appear that the surface renewal model is the more accurate way of characterising k for flows with significant bulk turbulence, which is mostly the case in the field. We cannot, however, simply ignore the strong correlations observed between k and the surface wave topology. In fact, it could very well be the case that we are looking at the two sides of the same coin here, as several studies have shown that the air-water interfacial topology is intricately linked with the underlying bulk turbulence properties (e.g. Brocchini & Peregrine, 2001; Savelsberg & van de Water, 2008, 2009; Smeltzer *et al.*, 2023). The difficulty arises when one tries to separate the two effects to perform systematic parametric studies. However, with the increasingly popular use of active turbulence grids, first pioneered by Makita (1991) and previously used in several wave-turbulence interaction investigations (Savelsberg & van de Water, 2008, 2009; Smeltzer *et al.*, 2023), such parametric studies can become practical. This study presents our effort to examine how surface wave topology and the bulk turbulence properties affect k separately. We drew inspirations from Adler (2022) to create the surface capillary waves through an array of dowels, and tailored the bulk turbulence through the use of an active grid. This allows us to create flow cases with similar surface topology but dissimilar bulk turbulence, and vice versa.

EXPERIMENTAL SET-UP

The experiments were conducted in the recirculating water channel at NTNU. The water channel has a test section measuring 1.0 m $\times$ 1.8 m $\times$ 11 m. We use x_1, x_2, and x_3 to represent the streamwise, vertical, and transverse directions, respectively. The water depth was maintained at $H \approx 0.23$ m, and the freestream velocity was $U_\infty = 0.42$ m s^{-1}. An active grid installed at the inlet of the test section is used to generate two different turbulence inflow conditions. The spacing between the centres of the rods, or mesh length, is $M = 0.1$ m. More details on the active grid and the water channel can be found in Jooss *et al.* (2021). For the first inflow condition (Static), the rods are held stationary with the wings feathered in the direction of the mean flow. For the second inflow condition (Active), each rod rotates at a frequency of $\Omega = 0.05$ Hz ± 0.025 Hz. The direction and duration of each rotation sequence are taken from a pre-generated randomized list. Several detailed active grid parametric studies have shown that if the grid Reynolds number $Re_M = U_\infty M/\nu$ is held constant, then Ω has the greatest influence over the turbulence inflow properties (e.g. Larssen & Devenport, 2011; Hearst & Lavoie, 2015).

An array of dowels, each with a diameter of 3.1 mm, was used to generate the surface capillary waves. The dowel array is made from stock construction nails hammered into wooden frames, and were positioned with a spacing of 0.06 m in x_1 and 0.15 m in x_3 between individual dowels. The entire array covers the region from $x_1 = 50M$ to $100M$ while spanning the width of the test section. Two submersion depths were tested: ~ 7.5 mm for the shallow case and ~ 70 mm for the deep case. Figure 1 shows an example of the surface capillary waves created by the dowel array.

The freestream turbulence in the liquid-phase, upstream of the dowel array, is characterized by laser Doppler velocimetry (LDV) through a FiberFlow dual-channel probe from Dantec Dynamics. The measurement point is placed 45M downstream from the active grid, in the centre of the channel at half water height (0.118 m). The acquisition frequencies are $O(100$ Hz$)$ for u_1 and $O(20$ Hz$)$ for u_3. The water is seeded with Dynoseeds TS-40 polystyrene particles with a nominal diameter of 40 μm.

A section of the flow field around the dowels is characterized by 2-D planar particle image velocimetry (PIV). A dual-pulse Litron Nano L Nd-YAG laser (200 mJ, 532 nm) is used to create a light sheet in the $x_1 - x_2$ plane, and a LaVision Imager MX 25 camera with a Zeiss 100 mm lens is used to capture the field. The field of view (FOV) measures 0.24 m $\times$ 0.24 m, and is centred at $x_1 = 85M$. A total of 3000 image pairs are taken for each case at 1 Hz, and vector field calculations are done through DaVis 10 with multiple passes, with the final pass using a 48×48 window with 50% overlap, resulting in a vector spacing of 1.14 mm.

The surface waves are characterized by a HR Wallingford resistive wave probe, with a sensing area of 1.6 mm $\times$ 15 mm. It is placed at $x_1 = 84.3M$, within the PIV's FOV but outside

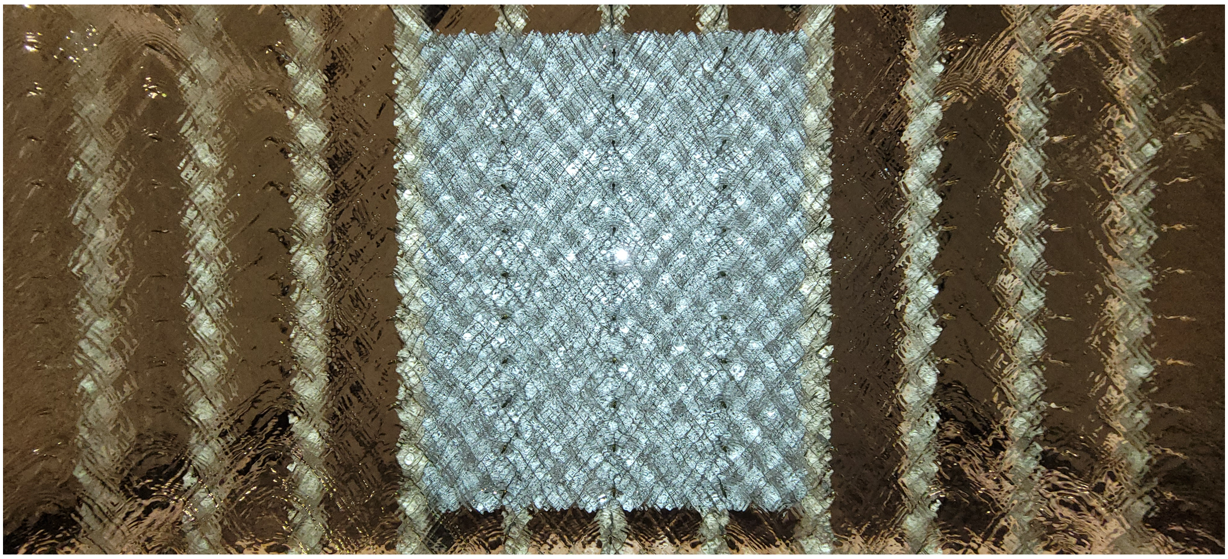

Figure 1: Example image showing the surface waves generated by the dowel array as viewed from below the test section through the glass floor. The flow is going from top to bottom.

of the actual measurement plane, and is oriented to measure the longitudinal waves. The vertical resolution of the probe is 0.1 mm. Probe calibration is performed prior to the start of each test case.

The dissolved bulk oxygen concentration (C_b) in the liquid-phase is measured by a PreSens O_2 & pH profiling microsensor. The sensor is placed at $x_1 = 85M$, but outside of the PIV measurement plane for the same reason as the wave gauge. The actual sensing point is at the tip of the sensor needle, placed ≈ 110 mm below the water surface. This is the maximum submersion depth for the sensor tip without incurring potential water damage to the rest of the sensor body. The original dissolved oxygen in the water is removed through the addition of sodium sulphite (Na_2SO_3), then oxygen is naturally re-dissolved into the water from the ambient lab air. C_b measurements are taken at 0.33 Hz until the water is fully saturated again, which takes on the order of 80 hours. To ensure that dissolved oxygen is first fully removed from the water before the experiment begins, the sensor is calibrated at the start of each test case, and its reading monitored until it plateaus at zero concentration. Throughout the subsequent re-aeration process, the water temperature and atmospheric pressure are measured concurrently along with the oxygen concentration. Plastic sheets are floated over the water surface for the entire facility except for where the dowel array is located, thus limiting gas transfer to only occur through the water surface underneath the array. The raw recordings of the oxygen concentration is post-processed to correct for ambient condition changes and sensor drift from its pre-experimental calibration. Using a PreSens proprietary software, 4000 points just before the initial C_b uptake and 4000 points at the end of the recording are taken as the zero and fully saturated O_2 concentrations, respectively, and all the recordings in between are re-scaled accordingly. This allows us to essentially perform *in-situ* calibrations of the O_2 probe at both ends of the concentration time-series.

In total, five test cases were investigated, covering different freestream turbulence levels and dowel depths. The configurations and inflow statistics are summarized in Table 1.

RESULTS & DISCUSSIONS

Figure 2 presents the turbulence intensity profiles u_1'/U_∞ in x_2 along with the power spectral density (PSD) and probability density functions (PDF) of the surface waves measured by the wave probe. It is evident in Figure 2a that the dowels introduce a significant addition to the velocity fluctuations through their solid blockage of the near surface flow. Even at shallow dowel depth (<10 mm penetration), the cumulative effects of the dowel array from $x_1 = 50M$ onward result in elevated velocity fluctuations ~ 86 mm below the surface, or about 10-dowel depths, for both the static and the active inflow conditions. On a relative term, the shallow dowels caused more deviations to the background u_1'/U_∞ profiles for the static case than the active case (cases REF & A vs. cases C & D). Interestingly, although the near surface velocity fluctuations for the active grid alone are higher than what is generated by the shallow dowels with static grid, the combination of dowels and active grid produced even higher velocity fluctuations. In other words, the active grid does not mask the effects of the shallow dowel array. The deep dowels (~ 70 mm penetration) caused the highest near surface velocity fluctuations out of all the cases, and their effects extend down to ~ 150 mm below the surface. The turbulence intensity near the surface for cases REF and A is approximately $4\% \pm 1\%$, while cases B, C, and D exhibit values of approximately $7\% \pm 1\%$. The bulk turbulence intensity, which we defined as u_{1b}'/U_b, is a more quantitative parameter for categorising the cases based on the bulk turbulence. The values for all cases are presented in Table 1. Here, $u_{1b}' = (\int u_1' \mathrm{d}x_2)/H$, and $U_b = (\int U_1 \mathrm{d}x_2)/H$ is the bulk velocity. This parameter gives a measure to the overall degree of turbulent fluctuations in the PIV field, and we can see again that cases REF and A have similar bulk turbulence intensities, while cases B, C, and D form another group of similar values.

The surface wave frequency content, illustrated in Figure 2b, demonstrates that both the grid and the dowels have significant impact. Comparing cases REF and C to just focus on the effect of the grid, we see that additional energy is introduced across all frequencies. Starting from the low frequencies, we see that the prominent peak near 0.04 Hz for case REF is amplified by two orders of magnitude with the addition of the grid. This peak is associated with the sloshing mode of the water channel. We make a note that although this peak also shows up in the active grid cases and it is very close to the grid activation frequency of 0.05 Hz, we do not believe that this is an imprint of the grid movement itself as the peak

Table 1: Test case configurations and statistics: u_1'/U_∞ and L_{11}/H are the freestream turbulence intensity and the normalized integral scale, respectively, measured by the LDV upstream of the dowels, h' is the RMS variation in the water surface height measured by the wave gauge, u_{1b}'/U_b is the bulk turbulence intensity integrated across the flow height, U_τ is the boundary layer friction velocity from the PIV measurements based on Rodríguez-López *et al.* (2015), and k is the gas transfer rate.

Case	Grid mode	Dowel config.	u_1'/U_∞ [%]	L_{11}/H	h' [mm]	u_{1b}'/U_b [%]	U_τ [mm s^{-1}]	k [cm h^{-1}]
REF	Static	None	3.2	0.05	0.11	4.9	16.6	31.2
A	Static	Shallow	3.2	0.06	0.41	5.2	17.0	34.7
B	Static	Deep	3.3	0.06	0.50	7.0	17.7	42.1
C	Active	None	9.0	1.01	1.12	7.2	17.9	44.7
D	Active	Shallow	8.8	1.01	1.21	7.3	18.2	45.2

is also prominent when the grid is off. On top of amplifying the sloshing mode, the active grid also significantly increased the wave fluctuations between 1 Hz and 20 Hz. Adding shallow dowels into the comparison (case A), we see that the peak associated with sloshing is masked, and there is also an overall increase in wave fluctuations across all frequencies compared to REF. Interestingly, for frequencies between 0.2 Hz and 5 Hz, the shallow dowels introduce more surface fluctuations to the baseline flow than the active grid, while the active grid is much more effective in amplifying fluctuations below 0.2 Hz. When we combine both the active grid and the shallow dowels (case D), we see that the frequency content of the fluctuations is quite similar to just the grid alone (case C), except for the region between 0.2 Hz and 5 Hz, where it is more similar to the shallow dowels (case A). Finally, the deep dowels (case B) produced surface fluctuations similar to that of the shallow dowels, with the main difference being that the deep dowels showed slightly higher fluctuations than the shallow dowels for $f > 4$ Hz, and the reverse is true for $f < 4$ Hz. The cumulative effects on the frequency content can be summarised by examining the RMS of the wave height time series h', as presented in Table 1. We can see that while there are some increases in h' from case REF to B, the most significant increase occurred when the grid was active (cases C & D). Furthermore, the difference in h' between the shallow and deep dowel cases is relatively small. Therefore, in terms of the frequency content of the surface waves, we can group cases A & B into one set, and cases C & D into another set, with case REF in a third set on its own.

The probability density functions of the wave heights in Figure 2c reveal that the two active grid cases have largely similar distributions, with case D exhibiting slightly wider tails due to the insertion of the dowels. The increased tails can be attributed to greater wave fluctuations between 0.2 Hz and 5 Hz as observed in the spectra. Conversely, cases A & B show similar profiles, where the increased dowel depth also produced larger tails. Regardless of the disturbance mechanism to the surface waves, both the dowel array and the active grid introduced significant intermittency to the surface wave fluctuations. A similar grouping between the cases based on the probability density functions can be made here, with cases A & B as one set, cases C & D as another set, and case REF in a third set.

Overall, regarding the average turbulence intensities, we can group cases REF & A into one set, and cases B, C, & D into another set. From a wave statistics perspective, the grouping can be arranged according to the grid settings. Thus, we have, to a certain degree, decoupled the surface wave and bulk turbulence properties.

Figure 3 illustrates C_b normalised by the saturation concentration C_s as a function of time. The data points are averaged over 15-minute windows. The saturation concentration C_s is computed from a look-up-table based on the works of Benson & Krause Jr (1980, 1984), with the input being the measured ambient temperature and the atmospheric temperature for each data point. It is evident that cases REF & A exhibit significantly slower C_b recovery rates compared to the other cases. The insertion of dowels at the shallow depth did enhance the recovery rate from the baseline REF case, but both the active grid and the deep dowel insertion resulted in significantly faster recovery rate for C_b. The fastest case appears to be case D, where shallow dowels are combined with the active grid. We have identified a region between $0.2 \leq C_b/C_s \leq 0.8$ after the initial C_b uptake for each case, which scales with $1 - e^{-k_L(t-t_0)}$ (e.g. Adler, 2022), where k_L and t_0 are fitting parameters. The fitted region is plotted in the left inset in Figure 3. To estimate k, we utilise $k = k_L V/A$, where V represents the total volume of the water as measured by a flow meter attached to the in-fill pipe, and A denotes the exposed air-water interface surface area beneath the dowel array (9 m^2). The computed values are presented in Table 1. A clear trend emerges, with k exhibiting a monotonic increase from case REF to D. Furthermore, we observe that cases REF & A share similar k values, around 33 cm h^{-1}, while cases B, C, & D show k clustered around 44 cm h^{-1}. This marks an increase of more than 30% from cases REF & A.

Computing U_τ from the PIV velocity profiles reveals insights into the physics behind this clustering of k. The parameter optimisation algorithm of Rodríguez-López *et al.* (2015) is applied to the PIV velocity profiles to estimate U_τ. The right inset in Figure 3 shows that k is strongly correlated with U_τ, consistent with the findings of Turney & Banerjee (2013). As U_τ is influenced by the cumulative effects of the bulk turbulence, it also correlates with the bulk turbulence properties (e.g. Hearst *et al.*, 2018), as can be seen in Table 1 between the values for u_{1b}'/U_b and U_τ. It can also be argued that the full velocity fluctuation profile $u_1'(x_2)/U_\infty$ near the end of the dowel array, represented by the bulk turbulence intensity, can be used directly to characterise the effects of bulk turbulence on k. We acknowledge that since this is a recirculating facil-

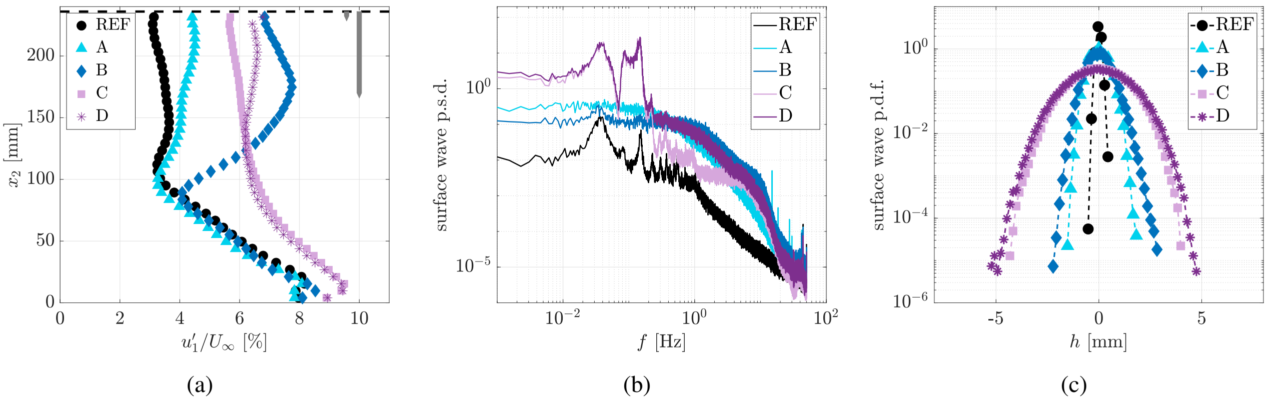

Figure 2: Characterisation of the flow field and surface waves showing (a) turbulence intensity profile (b) PSD and (c) PDF of the surface waves. The black dotted line in (a) represents the average water surface height, and the grey rods represent the dowel penetration depths.

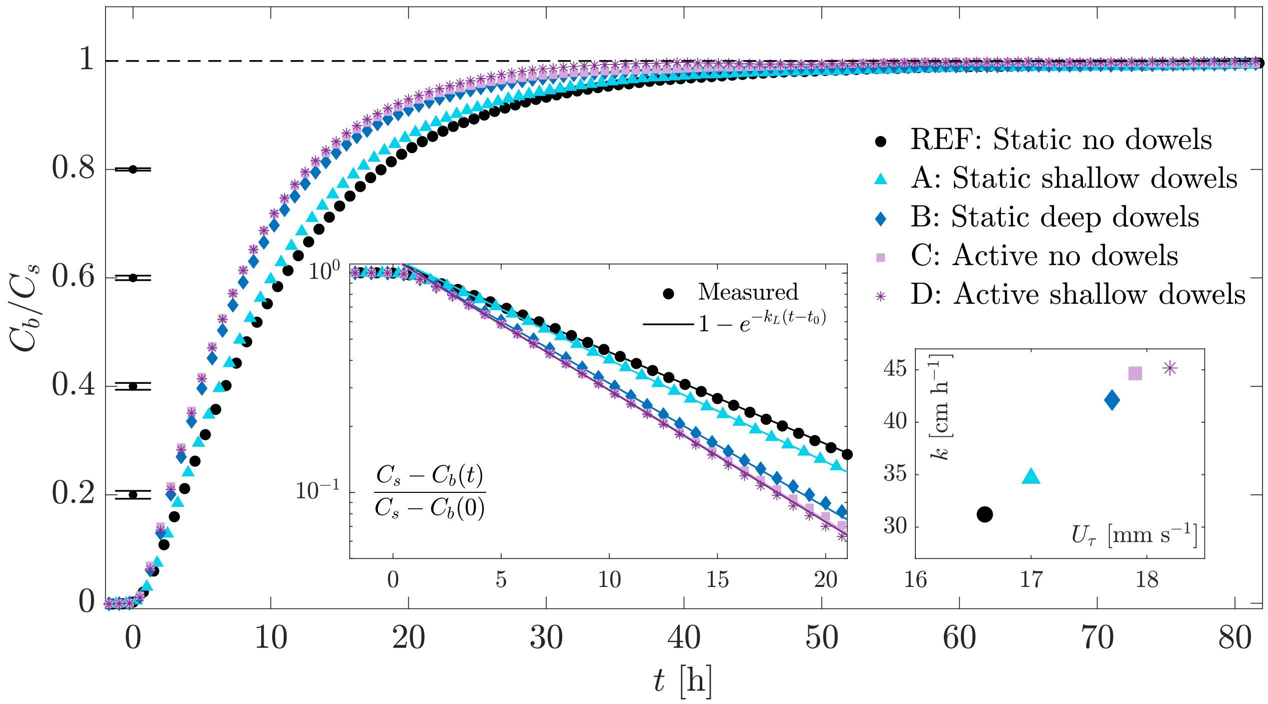

Figure 3: Normalized bulk concentration (C_b) for all test cases. The left inset shows the region where C_b/C_s scales with $1 - e^{-k_L(t-t_0)}$, while the right inset shows k vs. U_τ for all the test cases. The error bars to the left represent the worst case RMS variations of the 15-minute temporal averaging window at different C_b/C_s values.

ity, the water is mixed in the return loop and any differences in O_2 concentration in the water is likely homogenised once it returns to the start of the test section. However, plastic sheets covered all the exposed water surfaces except for those under the dowel array, and thus any mixing of the dissolved O_2 outside of the test section only acts upon the already dissolved O_2 in the water. This does not increase the bulk O_2 concentration significantly, but rather works to homogenise the concentration. New O_2 can only be absorbed through the surface under the dowel array into the bulk flow, which shows significant differences in velocity fluctuations profiles. The evidence presented here shows that elevated bulk turbulence intensity leads to a faster absorption of new oxygen into the water, thus increasing the C_b uptake rate.

Combining the results for all the test cases reveals distinct patterns. Cases A and B exhibit similar surface wave statistics, while their turbulence properties differ significantly, and we observe different k values. Conversely, cases B, C, and D display dissimilar surface wave statistics, but their turbulence properties are similar, and we observe similar k values despite the different turbulence generation mechanisms (dowel array vs. active grid). These observations strongly suggest that the bulk turbulence properties of the flow exert a greater influence on k than the surface capillary wave characteristics. Here we acknowledge that the past studies do show a strong correlation between the capillary wave characteristics and the gas transfer velocities. However, one cannot definitely say that they have isolated the effect of surface waves from the bulk turbulence as there was generally a lack of characterisation of the bulk flow. We have observed here that the insertion of dowels, even at a shallow depth, can cause significant elevations in velocity fluctuations well into the bulk flow. It stands to reason that other mechanisms for creating capillary waves, such as wind shear, can also lead to dispersion of the energy into turbulent fluctuations in the bulk flow. What we have shown here is that if two flows have similar surface characteristics but different bulk turbulence properties, the gas transfer velocity correlates with the bulk turbulence.

CONCLUSIONS

This study examined the impact of various surface capillary waves and bulk turbulence conditions on the transfer of O_2 across an air-water interface. The observed changes in the gas transfer rate k exhibited a stronger correlation with alterations in bulk turbulence properties than with changes in surface wave characteristics. These findings suggest that, at least within the tested parameters, bulk turbulence plays a more significant role than surface capillary waves in influencing the dissolution of low solubility atmospheric gases into water.

FUNDING

The work is co-funded by the Research Council of Norway (FRIPRO, *WallMix*, 288046) and the European Union (ERC StG, *GLITR*, 101041000). Views and opinions expressed are however those of the author(s) only and do not necessarily reflect those of the European Union or the European Research Council. Neither the European Union nor the granting authority can be held responsible for them.

REFERENCES

Adler, K. E 2022 Quantifying and parameterizing air–water gas transfer enhancement via capillary–gravity bow waves and streamwise counter–rotating vortices in environmental and industrial applications. PhD thesis, Cornell University.

Benson, B. B. & Krause Jr, D. 1980 The concentration and isotopic fractionation of gases dissolved in freshwater in equilibrium with the atmosphere. 1. oxygen. *Limnol. Oceanogr.* **25** (4), 662–671.

Benson, B. B. & Krause Jr, D. 1984 The concentration and isotopic fractionation of oxygen dissolved in freshwater and seawater in equilibrium with the atmosphere 1. *Limnol. Oceanogr.* **29** (3), 620–632.

Brocchini, M. & Peregrine, D. H. 2001 The dynamics of strong turbulence at free surfaces. part 1. description. *J. Fluid Mech.* **449**, 225–254.

Coantic, M. 1986 A model of gas transfer across air-water interfaces with capillary waves. *J. Geophys. Res.-Oceans* **91** (C3), 3925–3943.

Danckwerts, P. V. 1951 Significance of liquid-film coefficients in gas absorption. *Ind. Eng. Chem.* **43** (6), 1460–1467.

Hearst, R. J., Dogan, E. & Ganapathisubramani, B. 2018 Robust features of a turbulent boundary layer subjected to high-intensity free-stream turbulence. *J. Fluid Mech.* **851**, 416–435.

Hearst, R. J. & Lavoie, P. 2015 The effect of active grid initial conditions on high Reynolds number turbulence. *Exp. Fluids* **56**, 1–20.

Henstock, W. H. & Hanratty, T. J. 1979 Gas absorption by a liquid layer flowing on the wall of a pipe. *AIChE J.* **25** (1), 122–131.

Herlina, H. & Jirka, G. H. 2008 Experiments on gas transfer at the air–water interface induced by oscillating grid turbulence. *J. Fluid Mech.* **594**, 183–208.

Jähne, B., Münnich, K. O., Bösinger, R., Dutzi, A., Huber, W. & Libner, P. 1987 On the parameters influencing air-water gas exchange. *J. Geophys. Res.-Oceans* **92** (C2), 1937–1949.

Jirka, G. H., Herlina, H. & Niepelt, A. 2010 Gas transfer at the air–water interface: experiments with different turbulence forcing mechanisms. *Exp. Fluids* **49**, 319–327.

Jooss, Y., Li, L., Bracchi, T. & Hearst, R. J. 2021 Spatial development of a turbulent boundary layer subjected to freestream turbulence. *J. Fluid Mech.* **911**, A4.

Kanwisher, J. 1963*a* Effect of wind on CO_2 exchange across the sea surface. *J. Geophys. Res.* **68** (13), 3921–3927.

Kanwisher, J. 1963*b* On the exchange of gases between the atmosphere and the sea. In *Deep-Sea Res.*, , vol. 10, pp. 195–207. Elsevier.

Komori, Satoru, Nagaosa, Ryuichi & Murakami, Yasuhiro 1993 Turbulence structure and mass transfer across a sheared air–water interface in wind-driven turbulence. *J. Fluid Mech.* **249**, 161–183.

Larssen, J. V. & Devenport, W. J. 2011 On the generation of large-scale homogenous turbulence. *Exp. Fluids* **50**, 1207–1223.

Liss, P. S. 1973 Processes of gas exchange across an air-water interface. In *Deep-Sea Res.*, , vol. 20, pp. 221–238. Elsevier.

Longuet-Higgins, M. S. 1992 Capillary rollers and bores. *J Fluid Mech.* **240**, 659–679.

MacIntyre, F. 1971 Enhancement of gas transfer by interfacial ripples. *Phys. Fluids* **14** (8), 1596–1604.

Makita, H. 1991 Realization of a large-scale turbulence field in a small wind tunnel. *Fluid Dyn. Res.* **8** (1-4), 53.

McCready, M. J. & Hanratty, T. J. 1985 Effect of air shear on gas absorption by a liquid film. *AIChE J.* **31** (12), 2066–2074.

Rodríguez-López, E., Bruce, P. J. K. & Buxton, O. R. H. 2015 A robust post-processing method to determine skin friction in turbulent boundary layers from the velocity profile. *Exp. Fluids* **56**, 1–16.

Savelsberg, R. & van de Water, W. 2008 Turbulence of a free surface. *Phys. Rev. Lett.* **100** (3), 034501.

Savelsberg, R. & van de Water, W. 2009 Experiments on free-surface turbulence. *J. Fluid Mech.* **619**, 95–125.

Saylor, J. R. & Handler, R. A. 1997 Gas transport across an air/water interface populated with capillary waves. *Phys. Fluids* **9** (9), 2529–2541.

Saylor, J. R. & Handler, R. A. 1999 Capillary wave gas exchange in the presence of surfactants. *Exp. Fluids* **27** (4), 332–338.

Smeltzer, B. K., Rømcke, O., Hearst, R. J. & Ellingsen, S. Å. 2023 Experimental study of the mutual interactions between waves and tailored turbulence. *J. Fluid Mech.* **962**, R1.

Szeri, A. J. 1997 Capillary waves and air-sea gas transfer. *J. Fluid Mech.* **332**, 341–358.

Turney, D. E. & Banerjee, S. 2013 Air–water gas transfer and near-surface motions. *J. Fluid Mech.* **733**, 588–624.

Variano, E. A. & Cowen, E. A. 2013 Turbulent transport of a high-schmidt-number scalar near an air–water interface. *J. Fluid Mech.* **731**, 259–287.

Witting, J. 1971 Effects of plane progressive irrotational waves on thermal boundary layers. *J. Fluid Mech.* **50** (2), 321–334.

Woolf, David Kevin, Shutler, Jamie D, Goddijn-Murphy, Lonneke, Watson, AJ, Chapron, Bertrand, Nightingale, Philip D, Donlon, Craig J, Piskozub, J, Yelland, Margaret J, Ashton, Ian *et al.* 2019 Key uncertainties in the recent air-sea flux of CO_2. *Global Biogeochem. Cy.* **33** (12), 1548–1563.